

Distinct Mixing Regimes in Shallow Cumulus Clouds

Yael Arieli¹, Eshkol Eytan¹, Orit Altaratz¹, Alexander Khain², Ilan Koren¹

¹Department of Earth and Planetary Science, Weizmann Institute of Science, Rehovot, Israel

²Institute of Earth Science, Hebrew University, Jerusalem, Israel

Key Points:

- Three mixing regimes are identified using subsets of tracers with similar trajectories in the LES of a cumulus cloud.
- These mixing regimes persist throughout the cloud's lifetime, providing insights into cloud mixing dynamics.
- The dissipation stage of the cloud reveals cloud-top entrainment followed by down-drafts.

Corresponding author: Ilan Koren, Ilan.Koren@weizmann.ac.il

Corresponding author: Alexander khain, alexander.khain@mail.huji.ac.il

Abstract

Understanding the nature of mixing between cloudy air and its surroundings is an important and yet, open question. In this research, we use high-resolution (10m) bin-microphysics LES of a cumulus cloud, together with a Lagrangian passive tracer tracking method, to study mixing. We analyze the passive tracers as a function of their trajectories and the thermodynamic conditions they undergo inside and outside the cloud. Three main mixing regimes (core, periphery, and skin) are identified, each determining a subset of tracers with similar trajectories. These mixing regimes can be observed throughout the cloud's lifetime. At the dissipation stage, a fourth regime is identified: cloud-top entrainment followed by downdrafts.

Plain Language Summary

The mixing of shallow clouds with their environment is a key open question in climate research and prediction. This topic is challenging due to the complexity of cloud processes and the difficulty of accurately measuring and modeling them. This study uses high-resolution simulation and Lagrangian tracers to analyze mixing. The study identifies three different mixing regimes in Cumulus clouds throughout their lifetime. Each regime is characterized by specific types of tracer trajectories. A fourth regime is identified as part of the clouds' decay.

1 Introduction

How does a convective cloud mix with the non-cloudy environment surrounding it, and how does such mixing affect the cloud's properties? Mixing processes have raised long-lasting open questions in our understanding of cloud physics. Detrainment describes an outflow of cloudy air into the environment, while entrainment is an inflow of environmental air into the cloud. Both mixing types affect the clouds' microphysical and macrophysical properties, which dictate the clouds' lifetime, radiative properties, vertical fluxes, and precipitation. Fundamental questions about the origin of the in-cloud air (Heus et al., 2008; Paluch, 1979), how mixing affects droplet size distribution (Khain & Pinsky, 2018; Tölle & Krueger, 2014; Prabhakaran et al., 2020), and how clouds affect the environmental radiative properties (Eytan et al., 2020; Koren et al., 2007; Marshak et al., 2006) are still open. Moreover, a significant part of the discrepancy between climate model results is attributed to cumulus mixing parameterization (Rio et al., 2019; Villalba-Pradas & Tapiador, 2022). Hence, a better understanding of the mixing processes can significantly improve our climate understanding. Entrainment of environmental air into clouds tends to dilute the cloud and affect its buoyancy, thereby affecting the cloud mass vertical transport, while detrained air from the cloud tends to moisten and precondition the surrounding environment and change its dynamics (Lenderink et al., 2004; Tiedtke, 1989). Various entrainment and detrainment mechanisms have been suggested over the years. They included a mechanism of cloud-top entrainment followed by a penetrative downdraft (Squires, 1958), entrainment and detrainment induced by re-circulation vortex near the cloud-top (Blyth et al., 1988), and turbulence-based entrainment and detrainment flow from the cloud sides (Stommel, 1947). One way to study those mechanisms is by using Large Eddy Simulation (LES) models, which include detailed numerical treatment of the thermodynamics, radiation, and microphysics. This provides a high-resolution description of cumulus cloud processes and properties (A. Siebesma & Jonker, 2000). LES studies usually simulate a cloud field in a $25 - 100[m]$ resolution; in many studies, the high resolution combined with a large domain demanded simplified descriptions of the microphysical processes (bulk microphysics parametrization), known to affect cloud dynamics (Khain et al., 2015; Small et al., 2009). Some studies combined passive tracers with such LES models (Carpenter et al., 1998; Heus et al., 2008; Yeo & Romps, 2013; Zhao & Austin, 2005b, 2005a). The use of passive tracers allows us to study the entrainment in great detail, i.e., to examine the flow patterns of

entrained tracers and their life cycle within the cloud. Heus et al. (2008) used Lagrangian particle tracking in a cumulus cloud field. By plotting a probability map of the entrance level of the particles as a function of their exit level, they showed that almost all mixing occurs laterally and found no evidence for cloud-top entrainment. Moreover, they claimed that the cloud core is constantly diluted by lateral mixing. Heus and Jonker (2008) described the influence of this lateral mixing on the buoyant-driven subsiding shell. On the other hand, Zhao and Austin (2005a) showed that the vertical circulation at the cloud's upper part is the main driver of the cloud's mixing with its environment. Such circulation was later observed by a Doppler radar (Damiani et al., 2006; Wang & Geerts, 2015) and further studied using LES (Eytan et al., 2023; Romps & Charn, 2015; Sherwood et al., 2013; Strauss et al., 2022). These vortex-driven circulations are characterized by a strong ascending air in the cloud center, a strong divergence at the top, and subsidence at the edges. During the early stages of the cloud, these toroidal vortexes are characterized by coherent structures that dissipate as the cloud reaches its mature stage. Zhao and Austin (2005b) studied the vertical mass flux profiles of LES cumulus clouds and found the clouds to exhibit net downward mass transport at upper levels and net upward mass flux at lower levels. Further, the downward mass flux was driven by evaporation and occurred during dissipation. Although the above studies have provided many insights, there is still a gap in understanding cumulus cloud mixing processes and no general agreement about the relative importance of the different suggested mechanisms.

Clouds consist of adiabatic (undiluted) and non-adiabatic parts. The adiabatic fraction (AF) is a measure of adiabaticity and, hence, of mixing. The AF is defined as LWC/LWC_{ad} , where LWC_{ad} is the liquid water content that a parcel would gain while being lifted adiabatically from the cloud base. Eytan et al. (2021) tested different methods to calculate AF values by comparing them to an Eulerian passive tracer. Eytan et al. (2022) found that the adiabatic core of the cloud corresponded to $AF > 0.9$ and showed a $20 - 50[m]$ transition zone located near the cloud edge, characterized by $AF \leq 0.2$ and sharp microphysical gradients explained by turbulent mixing.

In this study, we use Lagrangian tracers to explore cloud mixing processes. We seed passive tracers that follow the airflow. The high-resolution (10m) LES-SBM model allows the passive tracer trajectories to describe air movements inside and outside the cloud in great detail. We use the AF as the main measure to capture the conditions that tracers experienced along their trajectories.

2 Methods

We used the **S**ystem for **A**tmospheric **M**odeling (SAM) (Khairoutdinov & Randall, 2003) coupled with the Spectral Bin Microphysical (SBM) scheme (Khain et al., 2004) to simulate trade cumulus clouds with the BOMEX case study setup (A. P. Siebesma et al., 2003; Friedman et al., 1970) and no horizontal background advection. The cloud was initiated by a thermal perturbation of $0.1[K]$. The aerosol concentration was set to $500cm^{-3}$ and distributed only below the cloud base ($600[m]$). The horizontal length of the domain was $5.12[km]$, with cyclic boundary conditions. The horizontal resolution of the simulation was $dx = dy = 10[m]$ and the vertical resolution $dz = 10[m]$ up to $3[km]$, and $50[m]$ for the upper-most kilometer (similar to the simulation in Eytan et al. (2021)). The simulation's time step was $dt = 0.5[sec]$, while the data was saved every $d\tau = 2[sec]$, meaning the temporal resolution of the Lagrangian tracking method was $d\tau = 2[sec]$. A cross-section of cloud liquid water content at different stages of its lifetime is presented in section S1 in the supplementary material.

All the Lagrangian calculations were performed offline using the output of the SAM simulation. ~ 1.2 million passive tracers were released at the time of cloud formation (at 23 minutes of simulation). The tracers were released in a cube of $\sim 400[m]$, centered around the cloud, between altitudes of 100 to $2000[m]$. The outer region, located more than $400[m]$

from the cloud center, was found to be a quiescent environment; hence, tracers were not seeded there.

Using the Eulerian velocity field, we calculated the trajectory of each tracer: $\frac{d\vec{r}}{dt} = \vec{u}(\vec{r}, t)$, where $\vec{u} = (u, v, w)$ is the Eulerian velocity field, and $\vec{r} = (x, y, z)$ is the tracer position vector.

The 3D velocity field was interpolated to a sub-voxel scale. Similarly, key thermodynamic and microphysical variables were interpreted, allowing us to describe the environmental conditions that each trajectory sampled.

Cloudy voxels were defined by a threshold of $LWC > 0.01[\frac{g}{kg}]$. The distance from the cloud edge (DFCE) was calculated using a horizontal Euclidean distance, while small cloud fragments that were not connected to the main cloud were deleted. Negative values of DFCE indicated tracers residing inside the cloud. To avoid uncertainties caused by the binary definition of a cloudy voxel and the grid size, a cloud entry (exit) event was considered only if the tracer had penetrated (crossed) a distance of more than $10m$ from the cloud edge. Figure 1 demonstrates one trajectory of a tracer seeded at 23 min, below the cloud base, at a $390[m]$ height. In panel a, the color represents the simulation run-time; in panel b, the color is the AF that the tracer passed while moving inside the cloud. Panel c shows a time series of the DFCE of one trajectory, and Panel d is a time series of the tracers' height. The tracer enters the cloud through its base, ascending within the cloud, and at 36 min, it starts to descend, finally exiting the cloud.

We use the best method for calculating the adiabatic fraction (AF) of shallow cumulus clouds (Eq.5 in Eytan et al. (2021), S1).

3 Results

To explore the mixing of the cloud with its environment, we analyze air transport into and out of the cloud. Thus, we follow tracers crossing the cloud boundaries in both directions. We present it on the entry-exit space (EES), spanned by the entry (y-axis) and exit (x-axis) elevations of all relevant trajectories at a given time window in the simulation. Chosen parameters are superimposed on the points marked on the EES using a color scale. Figure 2(a-c) presents the EES of the cloud growth stage. The times are limited to an exit time of 32 minutes (the time of the cloud's maximal top height). Each circle represents a single entry, indicating that a tracer can enter and exit more than once, and each passage through the cloud is represented by a circle in the figure. The color scale in Figure 2a represents the time (in minutes) the tracer spent inside the cloud, and in Figure 2b (c), the maximum (mean) AF the tracer passed while moving inside the cloud. Figure 2d is a density plot presented on a logarithmic scale. The maximal AF (AF_{max}) provides information about whether the tracers passed through the undiluted part of the cloud, and together with the mean AF (AF_{mean}), they provide information about the full trajectory.

Circles located at the lower triangle (below the diagonal) of the EES represent tracers that exit the cloud at a higher level than they enter it; hence, they ascend in the cloud. Circles located at the upper triangle represent tracers that descend in the cloud. The diagonal in the EES represents lateral mixing in which tracers enter and exit the cloud at a similar level.

Visual inspection of the EES structure in the upper panel of Figure 2 reveals several striking properties. First, the upper triangle is occupied only near the diagonal, meaning no significant in-cloud downdrafts have developed until this point in the cloud's lifetime. In addition, the density plot (Figure 2d) shows two high-density regimes, one along the diagonal and one at the lower horizontal part. These regimes also exhibit distinct properties of

the residence time and the AF values. These two regimes mark the borders of the lower triangle that behaves as a transition regime, showing smooth gradients of residence time and AF between the two high-density extremes. Each of the three distinct mixing regimes represents a unique dynamical behavior of a group of tracers:

1) The core-associated regime appears as the lower horizontal line on the EES. This regime is characterized by a high density of points and is confined by low-level tracers' entering points, high residence times, and high AF_{mean} and AF_{max} . It represents tracers that enter through the cloud base and ascend by the updraft to their exit height. They spend most of their in-cloud lifetime in the adiabatic core and only a short time in the diluted parts of the cloud before exiting it. This is denoted by the lower values of AF_{mean} compared to AF_{max} . This regime is associated with convective motion.

2) The skin-associated regime is the diagonal on the EES. This regime represents tracers that enter and exit the cloud at a similar height. It exhibits short residence times inside the cloud and low AF_{max} and AF_{mean} values. This regime is associated with small-scale turbulence at the skin of the cloud (tens of meters near the cloud edge).

3) The periphery-associated regime is the lower EES triangle confined by the regimes described above, marking a transition between their properties in both residence time and AF. Tracers in the periphery regime are entrained above the cloud base and ascend in the cloud upward to their exit level. This regime is associated with large-scale mixing that dilutes the cloud body.

Figure 3a is a schematic representation of the three regimes over the EES. The bottom panel in Figure 2 (panels e-h) depicts the same elements as in the upper one but without the requirement that the tracers exit the cloud within 32 min of simulation. It shows the level at which the tracer enters the cloud and its level in the cloud at 32 min. These panels are much denser, but the general picture is the same as in the upper panels. The fact that we can identify the same mixing regimes in both domains, as shown in the upper and bottom panels in Figure 2, validates and reinforces their existence.

The EES representing the tracers that enter and exit the cloud at the growth stage (Figure 2a-c) exhibits a relatively empty band just above the cloud base inflow. This reveals that tracers entrained within the cloud at its lower 100[m] tend to ascend up to ~ 200 [m] in the cloud. This sparsely occupied band may be associated with the entrainment driven by the toroidal vortex (Eytan et al., 2023; Zhao & Austin, 2005a). The toroidal vortex was suggested to play a key role in the large-scale mixing of clouds. While turbulence acts to enter ambient air, mostly to the cloud's skin (Eytan et al., 2022), the toroidal vortex dilutes the cloud's core by inducing strong entrainment at the lower part of the vortex (Eytan et al., 2023). As this vortex is situated in the upper part of the cloud, the entrainment at the lower part of the cloud is limited. So this sparse band separates the region near the cloud base (linked to the core) from the one above, which is most likely linked to the toroidal vortex. Figure S2 shows histograms of the vertical distance between the cloud-top height and the entrance level of tracers belonging to the periphery-associated mixing regime. These histograms show that when the cloud-top height is higher than 1400[m], the preferred entry height is ~ 450 [m] below it. This agrees with the toroidal vortex studies and the sparse band location on the EES.

Figure 3b provides additional information about the vertical displacement distribution in each mixing regime. We divide the data into three well-separated AF_{max} classes, according to the values detected on the EES: low $AF_{max} < 0.2$ in blue; medium $0.3 < AF_{max} < 0.8$ in yellow, and high $AF_{max} > 0.9$ in red. Note a discontinuity in the AF_{max} values for establishing a clear distinction between the three classes. The histograms present the vertical displacement of all tracers in each subset. The low AF_{max} set, related to the tracers in the skin-associated mixing regime, is distributed around a zero displacement, representing $\sim 12\%$ of the total entering-exiting trajectories. The medium AF_{max} set, linked to the periphery-associated mixing regime, represents $\sim 26\%$ of the tracers and exhibits mostly a moderate positive displacement, while the high AF_{max} subset constitutes $\sim 50\%$ of the tracers and shows a distribution of much larger positive displacements. The tracers that

entered the cloud from its base and crossed high AF_{max} values along their trajectory constitute $\sim 43\%$ of the total entries to the cloud that occurred before the 32 min of simulation. These tracers are part of the sub-cloud inflow and the core-associated mixing regime. Their average lifetime in the cloud is 4.6 ± 1.7 min. The other $\sim 57\%$ of the tracers entered the cloud above the cloud base and their average lifetime in the cloud is 2.3 ± 1.6 min.

We find that only $\sim 12\%$ of the tracers that entered the cloud above the base crossed high AF_{max} along their trajectories, meaning most of the tracers that laterally entered the cloud did not penetrate the adiabatic core.

To determine the time evolution of the mixing regimes as reflected on the EES, we examine it at three different time points. Around 29 min, the cloud is in its developing stage; at approximately 33 min, the cloud reaches its maximal vertical development; after that time, the sub-cloud updraft weakens, and the cloud starts to dissipate. Figure 4(a-f) shows the EES for the different stages. Panels a and d represent the tracers that exit the cloud at 29 to 30 min; panels b and e, between 33 and 34 min; and panels c and f, between 37 and 38 min. In this representation, no events are repeated in the different plots. Hence, each panel represents a different stage in the cloud's lifetime. Noticeably, the same mixing regimes can be recognized in all cloud stages, with the addition of some tracers on the upper triangle in the dissipation stage. The upper-right points in the graphs (Figure 4b,c,e,f) indicate an entrainment process in the upper part of the cloud, accompanied by in-cloud downdrafts.

The observed cloud-top entrainment at the dissipation stage agrees with the LES results of Carpenter et al. (1998) and Zhao and Austin (2005b). Those tracers that enter the upper part of the cloud descend several hundred meters ($dz < 700[m]$) within the cloud. This is consistent with the results in Zhao and Austin (2005b), where the cloud-top downdrafts occupy one-third of the cloud depth. The sinking air (caused by negative buoyancy at the inversion layer) drives the entrainment from the cloud top. The descended air from the top converges with the ascending air from the base, causing a horizontal divergence and detrainment (Eytan et al., 2023). This detrainment zone is evident as a more densely occupied rectangle in the right part of the graph (Figure 4e,f), indicating a pronounced detrainment at the cloud's upper $\sim 500[m]$. In fact, between minutes 37 and 38 (Figure 4f) $\sim 70\%$ of the tracers exit at the upper $500[m]$ of the cloud.

The updrafts at the upper part of the cloud weaken and turn into downdrafts at the dissipation stage, thereby allowing enhanced cloud-top entrainment. Just after the cloud reaches its maximal height (Figure 4b,e), downdrafts appear mostly at the edges of the cloud, as indicated by the moderate vertical displacement in the cloud and the small DFCE (Figure S3) of the data points above the diagonal. Later on, the downdrafts become stronger, as can be seen by the maximal AF, the DFCE, and the vertical displacement of the tracers above the diagonal.

4 Conclusions

In this study, we use a high-resolution Bin-microphysics LES of a single cloud together with Lagrangian tracer tracking to study mixing in cumulus clouds. The high-resolution simulation, coupled with a detailed microphysical scheme, provides a detailed description of the dynamic, thermodynamic, and microphysical fields. Moreover, it allows an accurate description of the tracers' trajectories in and out of the cloud. We tracked and analyzed the trajectories of ~ 1.2 million passive tracers while recording their location and surrounding microphysical and thermodynamic conditions.

We defined the tracers' entry-exit space (EES) by plotting their cloud entry level as a function of their exit level. We superimposed on this space a third dimension of another parameter (e.g., AF and residence time in the cloud). The EES, combined with the maximum

and mean AF (AF_{max}, AF_{mean}) and residence time, clearly reveal three types of trajectory mixing regimes. Each of the regimes represents a subset of tracer trajectories.

Tracers that are part of the core-associated mixing regime appear as a horizontal line of low-level entry on the EES. Those tracers have long residence times and high mean and maximum AF values. They enter the cloud through its base and ascend to higher exit levels. They spend most of their in-cloud time in the adiabatic core and only a short time in the outer (diluted) parts of the cloud before exiting it.

Tracers identified as part of the skin-associated mixing regime reside on the diagonal of the EES. This subset of tracers enters and exits the cloud at a similar height. It shows a short residence time in the cloud and low AF_{max} and AF_{mean} values. This type of tracers' trajectories can be associated with lateral mixing by small-scale turbulence on the cloud's outer layer. This is in agreement with Eytan et al. (2022), who used Eulerian analysis to show that the cloud's skin is characterized by $AF < 0.2$ and formed by turbulent mixing. This region was also studied by in-situ measurements (Gerber, 2000) and a toy model (Pinsky & Khain, 2018). Our new Lagrangian analysis confirms this hypothesis about turbulent mixing in the cloud skin by providing the actual motions of the tracers with their spatial and temporal scales rather than deducing it statistically.

The third regime is the periphery-associated mixing regime, a transition between the two above-mentioned regimes regarding residence time, AF_{max} , and AF_{mean} . These tracers enter the cloud above the base and penetrate deeper into the cloud, but most do not penetrate the adiabatic core (hence, they are characterized by moderate AF_{max} values). This finding does not agree with the interpretation of Heus et al. (2008) that the cloud core is constantly diluted by lateral mixing. It supports the existence of an undiluted core in cumulus clouds, which is a long-lasting debate in cloud physics (Eytan et al., 2022; Gerber et al., 2008; Pinsky & Khain, 2023; Romps & Kuang, 2010). The periphery-associated mixing regime has a nature of convective scale mixing; it is responsible for mixing ambient air into the body of the cloud and can be driven by a large-scale toroidal vortex (Eytan et al., 2023; Pinsky et al., 2023; Zhao & Austin, 2005a).

The three mixing regimes can be recognized at all stages of a cloud's lifetime. During the dissipation stage, we recognize the addition of cloud-top entrainment, followed by downdrafts and detrainment at lower levels. The detrainment layer designates the inversion layer when the cloud reaches its maximum height. Later, this detrainment layer descends as the cloud dissipates. Inversion layers are known to correlate with detrainment layers (Bretherton & Smolarkiewicz, 1989; Perry & Hobbs, 1996), which is often explained by deceleration of the ascending cloud top, horizontal divergence, and detrainment. Here, we show that a strong detrainment occurs during the dissipation stage while the cloud top descends (in agreement with Zhao and Austin (2005a) and Eytan et al. (2023)).

Our analysis suggests an interesting insight into the long-lasting debate about lateral vs. cloud-top mixing. In agreement with (Heus et al., 2008), who advocated lateral mixing, we show here that lateral mixing indeed dominates throughout the cloud lifetime. Part of the laterally entrained air is lifted higher in the cloud, and some enter and leave the cloud at a similar level. Regarding cloud-top mixing, we find clear evidence for cloud-top entrainment followed by downdrafts at the dissipation stage of the cloud life cycle. This enhances the decay of the cloud and seems to play an important role in the large outflow flux during the dissipation stage. These results agree with Carpenter et al. (1998) and Zhao and Austin (2005b).

5 Open Research

The SAM codes are available on the website: <http://rossby.msrc.sunysb.edu/~marat/SAM.html> The code and the data to reproduce the figures of the manuscript are publicly available at a repository: <https://doi.org/10.34933/0626fa0c-2507-4758-ba5d-955c644079be>

Acknowledgments

This project has received funding from the European Research Council (ERC) under the European Union’s Horizon 2020 research and innovation programme (CloudCT, grant agreement No 810370), and by The Israel Science Foundation (grants 2635/20; 1449/22).

References

- Blyth, A. M., Cooper, W. A., & Jensen, J. B. (1988). A study of the source of entrained air in montana cumuli. *Journal of Atmospheric Sciences*, *45*(24), 3944–3964.
- Bretherton, C. S., & Smolarkiewicz, P. K. (1989). Gravity waves, compensating subsidence and detrainment around cumulus clouds. *Journal of Atmospheric Sciences*, *46*(6), 740–759.
- Carpenter, R. L., Droegemeier, K. K., & Blyth, A. M. (1998). Entrainment and detrainment in numerically simulated cumulus congestus clouds. part iii: Parcel analysis. *Journal of the atmospheric sciences*, *55*(23), 3440–3455.
- Damiani, R., Vali, G., & Haimov, S. (2006). The structure of thermals in cumulus from airborne dual-doppler radar observations. *Journal of the atmospheric sciences*, *63*(5), 1432–1450.
- Eytan, E., Arieli, Y., Alexander, K., Pinsky, M., Altaratz, O., Gavze, E., & Koren, I. (2023). The role of the toroidal vortex in cumulus clouds’ entrainment and mixing. *submitted to Journal of Geophysics Research*.
- Eytan, E., Khain, A., Pinsky, M., Altaratz, O., Shpund, J., & Koren, I. (2022). Shallow cumulus properties as captured by adiabatic fraction in high-resolution les simulations. *Journal of the Atmospheric Sciences*, *79*(2), 409 - 428. Retrieved from <https://journals.ametsoc.org/view/journals/atsc/79/2/JAS-D-21-0201.1.xml> doi: 10.1175/JAS-D-21-0201.1
- Eytan, E., Koren, I., Altaratz, O., Kostinski, A. B., & Ronen, A. (2020). Longwave radiative effect of the cloud twilight zone. *Nature geoscience*, *13*(10), 669–673.
- Eytan, E., Koren, I., Altaratz, O., Pinsky, M., & Khain, A. (2021). Revisiting adiabatic fraction estimations in cumulus clouds: high-resolution simulations with a passive tracer. *Atmospheric Chemistry and Physics*, *21*(21), 16203–16217. Retrieved from <https://acp.copernicus.org/articles/21/16203/2021/> doi: 10.5194/acp-21-16203-2021
- Friedman, H. A., Conrad, G., & McFadden, J. D. (1970). Essa research flight facility aircraft participation in the barbados oceanographic and meteorological experiment. *Bulletin of the American Meteorological Society*, *51*(9), 822–835.
- Gerber, H. (2000). Structure of small cumulus clouds. In *Proc. 13th int. conf. on clouds and precipitation* (pp. 105–108).
- Gerber, H., Frick, G. M., Jensen, J. B., & Hudson, J. G. (2008). Entrainment, mixing, and microphysics in trade-wind cumulus. *Journal of the Meteorological Society of Japan. Ser. II*, *86*, 87–106.
- Heus, T., & Jonker, H. J. (2008). Subsiding shells around shallow cumulus clouds. *Journal of the Atmospheric Sciences*, *65*(3), 1003–1018.
- Heus, T., van Dijk, G., Jonker, H. J. J., & den Akker, H. E. A. V. (2008). Mixing in shallow cumulus clouds studied by lagrangian particle tracking. *Journal of the Atmospheric Sciences*, *65*(8), 2581 - 2597. Retrieved from <https://journals.ametsoc.org/view/journals/atsc/65/8/2008jas2572.1.xml> doi: 10.1175/2008JAS2572.1
- Khain, A., Beheng, K., Heymsfield, A., Korolev, A., Krichak, S., Levin, Z., . . . others (2015). Representation of microphysical processes in cloud-resolving models: Spectral (bin) microphysics versus bulk parameterization. *Reviews of Geophysics*, *53*(2), 247–322.

- Khain, A., & Pinsky, M. (2018). *Physical processes in clouds and cloud modeling*. Cambridge University Press.
- Khain, A., Pokrovsky, A., Pinsky, M., Seifert, A., & Phillips, V. (2004). Simulation of effects of atmospheric aerosols on deep turbulent convective clouds using a spectral microphysics mixed-phase cumulus cloud model. part i: Model description and possible applications. *Journal of the Atmospheric Sciences*, 61(24), 2963–2982. Retrieved from <https://journals.ametsoc.org/view/journals/atasc/61/24/jas-3350.1.xml> doi: 10.1175/JAS-3350.1
- Khairoutdinov, M. F., & Randall, D. A. (2003). Cloud resolving modeling of the arm summer 1997 iop: Model formulation, results, uncertainties, and sensitivities. *Journal of Atmospheric Sciences*, 60(4), 607–625.
- Koren, I., Remer, L. A., Kaufman, Y. J., Rudich, Y., & Martins, J. V. (2007). On the twilight zone between clouds and aerosols. *Geophysical research letters*, 34(8).
- Korolev, A. V., & Mazin, I. P. (2003). Supersaturation of water vapor in clouds. *Journal of the Atmospheric Sciences*, 60(24), 2957–2974. Retrieved from https://journals.ametsoc.org/view/journals/atasc/60/24/1520-0469.2003.060_2957_sowvic_2.0.co_2.xml doi: 10.1175/1520-0469(2003)060<2957:SOWVIC>2.0.CO;2
- Lenderink, G., Siebesma, A. P., Cheinet, S., Irons, S., Jones, C. G., Marquet, P., . . . others (2004). The diurnal cycle of shallow cumulus clouds over land: A single-column model intercomparison study. *Quarterly Journal of the Royal Meteorological Society: A journal of the atmospheric sciences, applied meteorology and physical oceanography*, 130(604), 3339–3364.
- Marshak, A., Platnick, S., Várnai, T., Wen, G., & Cahalan, R. F. (2006). Impact of three-dimensional radiative effects on satellite retrievals of cloud droplet sizes. *Journal of Geophysical Research: Atmospheres*, 111(D9).
- Paluch, I. R. (1979). The entrainment mechanism in colorado cumuli. *Journal of the atmospheric sciences*, 36(12), 2467–2478.
- Perry, K. D., & Hobbs, P. V. (1996). Influences of isolated cumulus clouds on the humidity of their surroundings. *Journal of the atmospheric sciences*, 53(1), 159–174.
- Pinsky, M., Eytan, E., Gavze, E., & Khain, A. (2023). Vortex structure of head bubble in convective cloud starting plume. *Journal of the Atmospheric Sciences*.
- Pinsky, M., & Khain, A. (2018). Theoretical analysis of the entrainment–mixing process at cloud boundaries. part i: Droplet size distributions and humidity within the interface zone. *Journal of the atmospheric sciences*, 75(6), 2049–2064.
- Pinsky, M., & Khain, A. (2023). Convective and turbulent motions in nonprecipitating cu. part iii: Characteristics of turbulence motions. *Journal of the Atmospheric Sciences*, 80(2), 457–471.
- Prabhakaran, P., Shawon, A. S. M., Kinney, G., Thomas, S., Cantrell, W., & Shaw, R. A. (2020). The role of turbulent fluctuations in aerosol activation and cloud formation. *Proceedings of the National Academy of Sciences*, 117(29), 16831–16838.
- Rio, C., Del Genio, A. D., & Hourdin, F. (2019). Ongoing breakthroughs in convective parameterization. *Current Climate Change Reports*, 5(2), 95–111.
- Romps, D. M., & Charn, A. B. (2015). Sticky thermals: Evidence for a dominant balance between buoyancy and drag in cloud updrafts. *Journal of the Atmospheric Sciences*, 72(8), 2890–2901.
- Romps, D. M., & Kuang, Z. (2010). Do undiluted convective plumes exist in the upper tropical troposphere? *Journal of the Atmospheric Sciences*, 67(2), 468–484.
- Sherwood, S. C., Hernández-Deckers, D., Colin, M., & Robinson, F. (2013). Slippery thermals and the cumulus entrainment paradox. *Journal of the Atmospheric Sciences*, 70(8), 2426–2442.
- Siebesma, A., & Jonker, H. (2000). Anomalous scaling of cumulus cloud boundaries. *Physical review letters*, 85(1), 214.
- Siebesma, A. P., Bretherton, C. S., Brown, A., Chlond, A., Cuxart, J., Duynkerke, P. G., . . . Stevens, D. E. (2003). A large eddy simulation intercomparison study of shal-

- low cumulus convection. *Journal of the Atmospheric Sciences*, 60(10), 1201 - 1219. Retrieved from https://journals.ametsoc.org/view/journals/atasc/60/10/1520-0469_2003_60_1201_alesis_2.0.co_2.xml doi: 10.1175/1520-0469(2003)60<1201: ALESIS>2.0.CO;2
- Small, J. D., Chuang, P. Y., Feingold, G., & Jiang, H. (2009). Can aerosol decrease cloud lifetime? *Geophysical Research Letters*, 36(16).
- Squires, P. (1958). Penetrative downdraughts in cumuli. *Tellus*, 10(3), 381–389.
- Stommel, H. (1947). Entrainment of air into a cumulus cloud. *J. Meteor*, 4(3), 91–94.
- Strauss, C., Ricard, D., & Lac, C. (2022). Dynamics of the cloud–environment interface and turbulence effects in an les of a growing cumulus congestus. *Journal of the Atmospheric Sciences*, 79(3), 593–619.
- Tiedtke, M. (1989). A comprehensive mass flux scheme for cumulus parameterization in large-scale models. *Monthly weather review*, 117(8), 1779–1800.
- Tölle, M. H., & Krueger, S. K. (2014). Effects of entrainment and mixing on droplet size distributions in warm cumulus clouds. *Journal of Advances in Modeling Earth Systems*, 6(2), 281–299.
- Villalba-Pradas, A., & Tapiador, F. J. (2022). Empirical values and assumptions in the convection schemes of numerical models. *Geoscientific Model Development*, 15(9), 3447–3518.
- Wang, Y., & Geerts, B. (2015). Vertical-plane dual-doppler radar observations of cumulus toroidal circulations. *Journal of Applied Meteorology and Climatology*, 54(10), 2009–2026.
- Yeo, K., & Romps, D. M. (2013). Measurement of convective entrainment using lagrangian particles. *Journal of the Atmospheric Sciences*, 70(1), 266 - 277. Retrieved from <https://journals.ametsoc.org/view/journals/atasc/70/1/jas-d-12-0144.1.xml> doi: 10.1175/JAS-D-12-0144.1
- Zhao, M., & Austin, P. H. (2005a). Life cycle of numerically simulated shallow cumulus clouds. part ii: Mixing dynamics. *Journal of the atmospheric sciences*, 62(5), 1291–1310.
- Zhao, M., & Austin, P. H. (2005b). Life cycle of numerically simulated shallow cumulus clouds. part i: Transport. *Journal of the Atmospheric Sciences*, 62(5), 1269–1290.

Figure 1. An example of one trajectory. The cloud mask (in grey) represents the cloud structure at 32 min. a) A 3D trajectory of one tracer, the color scale marks the simulation run-time, b) The same as **a**, but the color scale represents the AF, and the cloud is presented from a different angle. c) The distance of the tracer from the cloud edge as a function of time. d) The vertical height of the tracer as a function of time. The blue (green) vertical dashed lines in panels **c-d** mark the time of the tracer entering (exiting) the cloud. The grey vertical lines represent the uncertainty zones where the tracer is near the cloud edge, penetrating a distance of less than 10[m].

Figure 2. Panels **a-d**: The height at which each tracer entered the cloud as a function of the exit height. Panels **e-h**: the height at which each tracer entered the cloud as a function of its height at 32 min of simulation (mature stage). The color scale in panels **a,d** represents the time [min] the tracer spent inside the cloud. The color scheme in panels **b,f/c,g** represents the maximum/mean AF the tracer passed inside the cloud. Panel **d/h** is a probability plot on a logarithmic scale (representing 46, 189 / 233, 417 tracers).

Figure 3. (a) Schematic of the three mixing regimes on the TEE space. The colors represent the mixing regimes: blue for the skin, yellow for the periphery, and red for the core regime. (b) Histograms of the vertical displacements that tracers undergo in the cloud while passing through maximum AF values of: blue) $AF_{max} < 0.2$, yellow) $0.3 < AF_{max} < 0.8$, and red) $AF_{max} > 0.9$. N is the number of tracers in each subset.

Figure 4. Time evolution. Entry height as a function of the exit height for each tracer that entered and exited the cloud. The colors at the top row represent the time inside the cloud, and at the bottom row, the maximum AF inside the cloud. In panels **a,d**, the entry occurs before the simulation run-time of 30 min, and the exit is at 29 to 30 min simulation time. In panels **b,e**, the entry is before 34 min, and the exit is at 33 to 34 min. In panels **c,f**, the entry is before 38 min, and the exit is between 37 to 38 min.

Figure1.

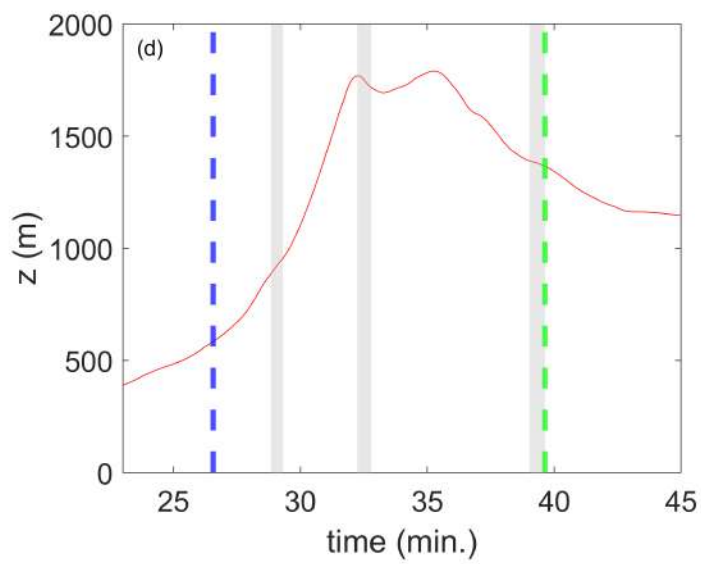
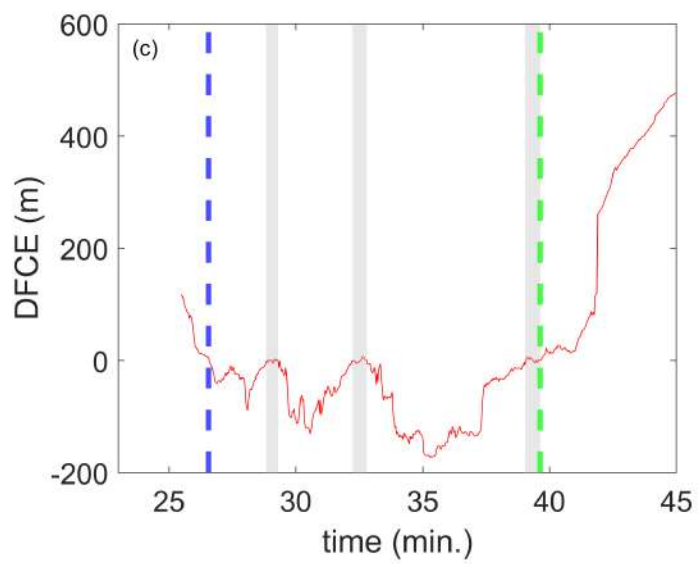
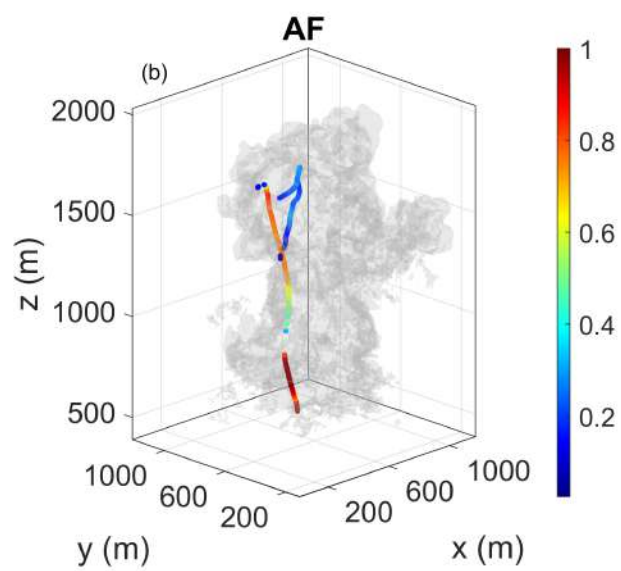
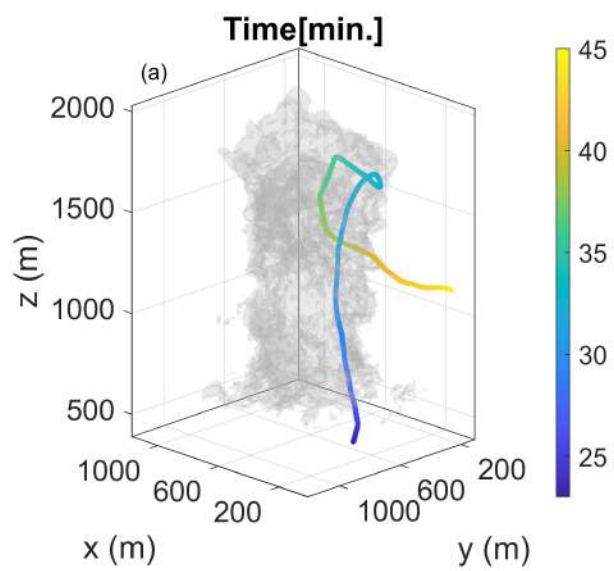


Figure 2.

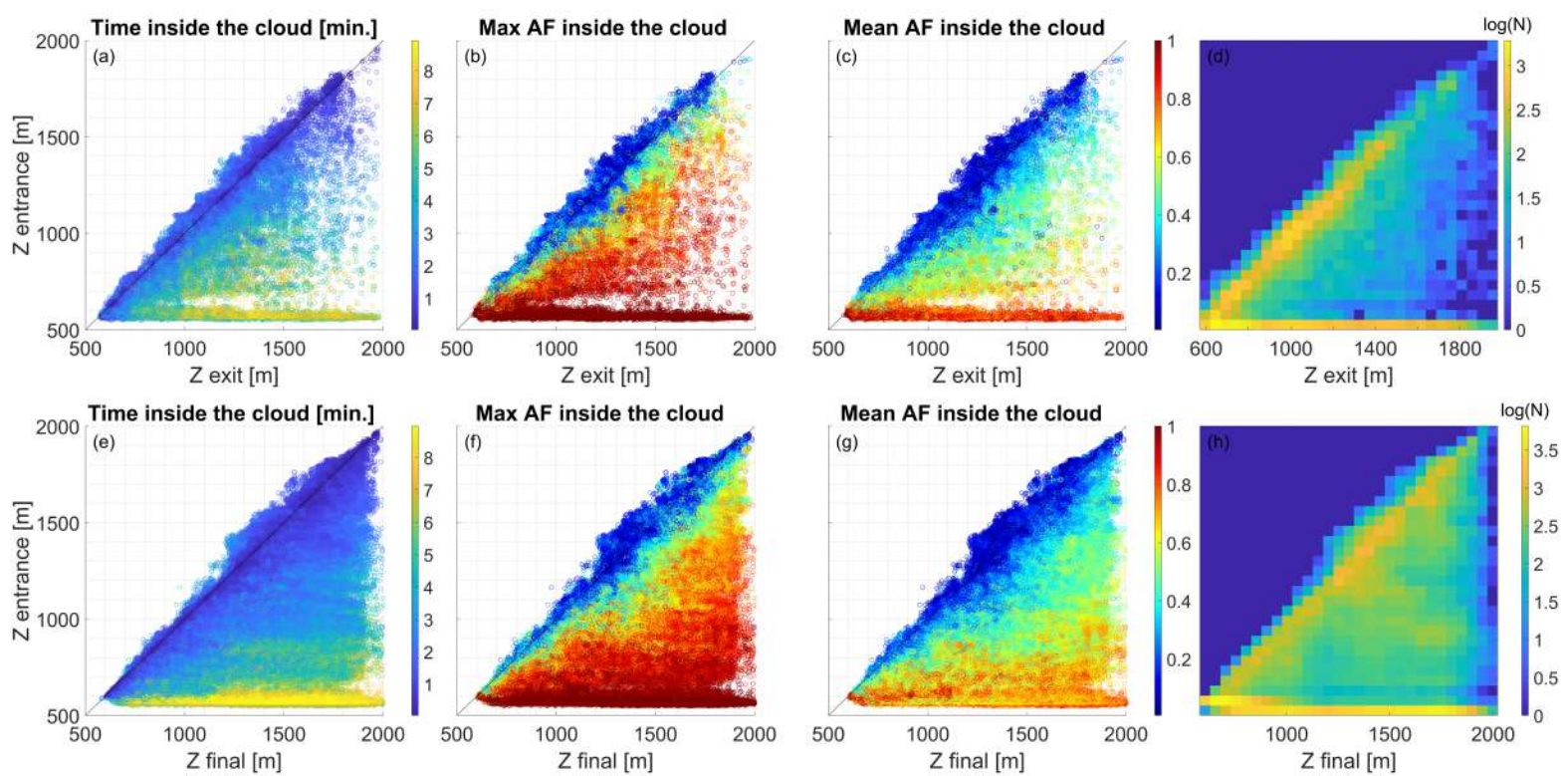


Figure 3.

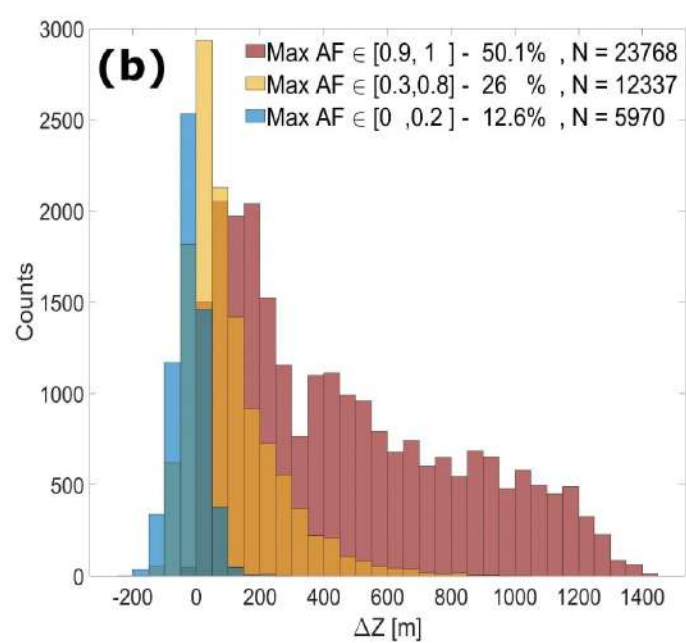
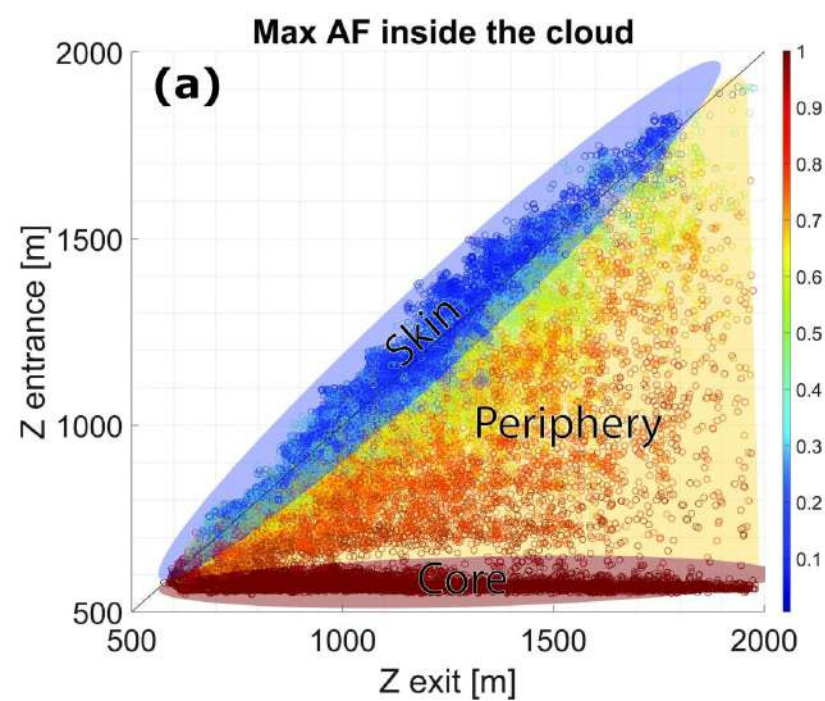


Figure 4.

